

Ship- and island-based atmospheric soundings from the 2020 EUREC⁴A field campaign

Claudia C. Stephan¹, Sabrina Schnitt⁸, Hugo Bellenger¹³, Simon de Szoek¹², Hauke Schulz¹, Katharina Baier^{1,*}, Tobias Böck^{8,*}, Thibaut Dauhut^{1,*}, Estefanía Quiñones Meléndez^{12,*}, Claudia Acquistapace^{8,+}, Gholamhossein Bagheri^{9,+}, Alton Daly^{6,+}, Nicolas Geyskens^{15,+}, Johannes Güttler^{9,+}, Kevin Helfer^{3,+}, Friedhelm Jansen^{1,+}, Alex Kellman^{7,+}, Sebastian Loss^{4,+}, Yanmichel Morfa-Avalos^{1,+}, Almuth Neuberger^{1,+}, Renaud Person^{14,+}, Andreas Reake^{11,+}, Maximilian Ringel^{2,+}, Markus Ritschel^{16,+}, Johannes Röttenbacher^{5,+}, Pauline Sadoulet^{18,+}, Imke Schirmacher^{2,+}, Katharina Stolla^{2,+}, Richard Wilson^{17,+}, Ethan Wright^{19,+}, Sandrine Bony¹³, and Bjorn Stevens¹

¹Max-Planck Institute for Meteorology

²University of Hamburg

³TU Delft

⁴University of New Mexico

⁵University of Leipzig

⁶CIMH

⁷Barbados Coast Guard

⁸University of Cologne

⁹Max Planck Institute for Dynamics and Self-Organization, Göttingen

¹¹DWD ?

¹²Oregon State

¹³Laboratoire de Météorologie Dynamique

¹⁴Institute of Research for Development, OSU, Ecce Terra, Laboratoire d’Océanographie et du Climat

¹⁵Centre national de la recherche scientifique

¹⁶no info

¹⁷Sorbonne Université, LATMOS, Paris, France

*These authors contributed equally to this work.

+These authors contributed equally to this work.

¹⁸Météo-France

¹⁹Florida State University

Correspondence: Claudia C. Stephan (claudia.stephan@mpimet.mpg.de)

Abstract. TEXT

Copyright statement. TEXT

1 Introduction

TEXT

5 2 Data collection

2.1 Measurement strategy

Between Jan xx and Feb xx, a total number of YYY radiosondes of type RS41-SGP produced by Vaisala were successfully launched from four research vessels and from the Barbados Cloud Observatory (BCO). The fleet of ships consisted of the two German research vessels Maria S. Merian (MS-Merian) and Meteor, the French vessel Atalante and ...Ronald H. Brown.

10 All ships are top class research facilities. The BCO The number of launches per day as well as the dates of data coverage differ from platform to platform. This was necessary to match time constraints, such as the availability of the ships, as well as to support individual research interests associated with specific platforms. Taking these boundary conditions into account, we designed the radiosonde network and measurement strategy to optimize the joint contribution of all platforms to the overarching goals of EUREC^{4A}. One specific goal was the characterization of the large-scale circulation. For this purpose it would be

15 optimum if the five stations were situated at the corners of a pentagon. The Meteor remained nearly stationary at a longitude of 57°W moving south and north between xx – °N to support coordinated aircraft measurements in the vicinity. The RH-Brown followed a trajectory that is approximately orthogonal to Meteor's sampling line, moving between the BCO and the NTAS buoy at xx.xx. The RH-Brown thus sampled airmasses in the upwind direction of the BCO that move westward with the predominant easterly trade winds in the latitude band 12.5-14.5, which is also referred to as the 'Trade Wind Alley' in the

20 context of the EUREC4A field campaign. The MS-Merian and Atalante ventured southward to a minimum latitude of xxN to capture oceanic and atmospheric variability associated with ocean eddies that move northward off the coastline of South America. When spatially well-separated, the MS-Merian and Atalante thus form the southern two corners of the radiosonde network. On these occasions we aimed at 4-hourly soundings from all platforms, reducing the number when separation was not maintained or when vessels left the key region of the network, i.e. moved south of 12N. These latter scenarios occurred

25 from time to time in order to support other measurements.

To increase the number of vertical profiles we recorded the ascent as well as the descent of the instruments. Except for the RH-Brown the balloons were equipped with parachutes to avoid excessively large fall velocities. Given that the combined time of ascent plus descent can take up to xxx hours, the sampling can be considered nearly continuous. All platforms deploy radiosondes of type Vaisala RS41-SGP and use the same software, MW41 by Vaisala, to record and process the sounding data.

30 In advance of the field campaign we organized a field day so people from different platforms could be trained at launching sondes and using the software. The basic steps of sonde preparation are the same for all platform. After a sonde is removed from the airtight foil the software calibrates the instrument by performing an automated initialization procedure, which takes about 5–6 min. In the meantime the frequency at which the sonde transmits its signal to the receiver is set manually to a predefined frequency (listed in Table A1).

35 We decided on standard launch times at 0245, 0645, 1045, 1445, 1845, and 2245 UTC. Departures from this schedule occurred due to a variety of reasons, including defective sondes, balloon bursts before the launch, collisions of ascending sondes with other onboard instrumentation or a lack of launch authorization in some regions.

Some aspects of the launch procedure as well as the problems that were encountered are specific to each platform. We list them in following.

40 2.2 Platform-specific procedures and problems

2.3 BCO

The BCO is located at the eastern-most point of Barbados (13.16°N , 59.43°W) and thus directly exposed to the easterly trade winds. Radiosondes were prepared inside an air-conditioned office container with air temperature and relative humidity adjusted to 20°C and 60%, respectively. Balloons were prepared outside and placed into a launcher whose size provided rough guidance for achieving the desired filling level. Air Traffic Control had to grant permission for every launch, which caused delays of up to 15 min. Surface conditions obtained from the weather station observations at BCO were entered into the software after automatic release detection. Data in BUFR format were automatically transmitted to the Global Telecommunication System (GTS) when the instruments reached 100hPa, at the end of ascent, and end of descent; no transmission was possible on some days due to network issues at BCO.

50 2.4 Meteor

Radiosondes were prepared inside a laboratory on the top of the ship with the antenna placed on the roof. Before February 9 the instruments were launched from the container of the German Weather Service (DWD), which is located on the backboard side at the back of the ship (Fig. X). This container has a ball marker for the optimum fill level of the balloons.

On February 9 the DWD launcher broke and the Meteor scientists started using a launcher such as the one shown in Fig. 55 X at the back of the ship (height ~2 m). An awning over the balloon indicated the fill level. Ground data were obtained from measurements taken by the DWD. These consisted of 10-min averages of pressure (sensor at 11.2 m above MSL), temperature and relative humidity (29.1 m), wind speed (25.3 m) and wind direction (35.0 m). In addition to the EUREC4A science crew, the DWD launched one radiosonde per day at around 16:33 UTC. These data are included in our level-2 and level-3 data sets (29 ascending soundings in total, launched between 16:30 and 17:00 UTC).

60 2.5 RH-Brown

NOAA Ship Ronald H. Brown, part of the NOAA's Marine Operations Center – Atlantic (MOC-A) fleet, is a Global Class research vessel that has been in service since 1997.

Radiosondes were prepared inside a strongly air-conditioned interior laboratory space. Afterwards they were taken to the main aft deck and placed on a convenient object, such as a chair or work box in the shade, to equilibrate to ambient environmental conditions for 1-5 minutes. Surface measurements were obtained from the ships meteorological data. The software writes Vaisala proprietary .mwx binary files, as well as BUFR 309052 (ascent) and 309053 (descent) messages.

On leg 1 at night, less helium and buoyancy of the balloon was used to achieve lower ascent rate, sample smaller scales in the atmosphere. The same target ascent rate was used for daylight and night in leg 2.

Soundings were emailed in multiple batches 2-3 times per day to the US national weather service to enter the GTS, but we
70 could not find out which particular soundings made it to the GTS.

2.6 Atalante

The sondes were prepared at the rear of the bridge. This open space is right next to the top building of the ship, which may affect measurements at low levels. Before the launch, operators asked the bridge for direction change if necessary and possible, and went outside to launch the sonde with the balloon.

75 The balloons were launched by hand, just next to the rear-bridge, where the helium and the launcher were installed. The Vaisala and Meteomodem antennas were installed on the roof top. The launcher size served as a reference for the Helium fill level. Surface measurements were obtained from local measurements onboard. At the beginning a frequency of 401 MHz was selected for sondes, which then had to be switched to 401.2 MHz because of the reception of a signal at 400.9 MHz from an unknown source which was suspected to interfere with two launched sondes and caused lost signals during the ascent. When a
80 previous sounding was not terminated at the launch time of a subsequent sounding, a frequency of 400.7 MHz was selected.

The Atalante experienced substantial instabilities of the Vaisala acquisition system at the initialization step of the system (system location unavailable) and with the reception the GPS signal by the Vaisala antenna and sondes. These problems required multiple restarts of the software and the aquisition system (between 1 and 8 times), creating delays between 10 min and 1 h. However, they did not affect the quality of the soundings. The operators checked the cables and replaced the GPS antenna
85 of the Vaisala system with an antenna that had a larger DC voltage range (15 V instead of 4 V). Nevertheless, the problems persisted during the cruise with the necessity to restart the system several times before each launch.

A coordinated sounding phase was performed with the MS-Merian to increase the temporal resolution from 3Jan 30 at 2045 UTC to Feb 2 at 16h45 UTC. During this time launching times were shifted by 2 hours onboard the Atalante (0045, 0445, 0845, 1245, 1645, 2045 UTC) whereas the MS- Merian launched at regular times. Files in BUFR format were generated for
90 each recorded ascent and descent and sent by email to Météo-France for data assimilation into the meteorological forecasting models through the GTS.

2.7 Merian

The Helium fill level was decided by inflating the balloon until it reached the upper edge of the launch container. The air conditioning inside the room, located on 2nd floor on the rear of the boat, was broken and it was hot inside. Many sondes from
95 the Merian did not reach the 100 hPa level for unknown reasons. Adjusting the amount of Helium did not make a difference. Surface data were taken from local ship measurements. The operators reported that the Helium pressure reduction did not properly work during the first half of the cruise. It was leaking and did not reduce the pressure sufficiently. It was replaced later on. A more severe problem was that the Merian did not receive descending data most of the time. The radio signal was lost prematurely, a few times even after several minutes after launch. The team tried to move the antenna from the top of the launch
100 container to another container but this did not help.

2.8 Quality control and data formats

We provide data at three levels: level-2 are QC data in NetCDF format, level-3 data ...In addition we provide the raw output (level-0).

2.8.1 level-2 data

105 In order to have a common dataformat to exchange the sounding data among meteorologists but also to send it to the GTS during the campaign, we agreed on the BUFR file format. Besides the support for dropsonde data (BUFR 309053) and traditional soundings (BUFR 309057), it supports also descending radiosondes (BUFR 309056) since BUFR Table version 31.0.0. These BUFR files are quality checked and created via the Vaisala MW41 sounding software. The Vaisala quality control algorithm detects outliers in the profiles and performs a smoothing to reduce noise. Missing data are interpolated to arrive at a continuous
110 profile.

The Sounding System MW41 performs a time lag correction algorithm. At 10 hPa the response time is 2.5 s for a speed of 6 m/s. For example, at 18 km (75 hPa) with a temperature lapse rate of 0.01°C/m and an ascent rate varying from 3 to 9 m/s, the remaining uncertainty in the temperature reading due to time lag is 0.02°C (k=2). At lower altitudes the uncertainty is even smaller.

115 A radiation correction is applied to daytime temperature measurements by subtracting increments that vary as a function of pressure and solar zenith angle. The uncertainty of the radiation correction is typically less than 0.2°C (k=2) in the troposphere; uncertainty gradually increases in the stratosphere.

A time-lag correction is also applied to measurements of humidity. The sensor heating capability enables active de-icing during sounding.

120 Nevertheless, for the scientific work the netCDF format is the preferred format in our community. Our software (http://github.com/observingClouds/eurec4a_snd) uses the ecCodes library (<https://github.com/ecmwf/eccodes>) to read the BUFR files and outputs the data to a netCDF file. In order to output the originally measured relative humidity instead of the dew point temperature, the inverse of the formula that the Vaisala MW41 software uses to calculate the dew-point temperature from the relative humidity has been applied.

125 In addition, the ascent-rate is calculated as the fraction of the gradient of the geopotential height and the passed time between two measurements.

2.8.2 level-3 data

For an easier scientific analysis the data has been interpolated in a further step onto a common altitude grid (10m spacing). While the interpolation of temperature, wind speed, wind direction and position are linear and straightforward, the interpolation
130 of relative humidity and pressure is more demanding.

In case of the relative humidity we calculated the water vapor mixing ratio (based on the Vaisala reported dew-point temperature and the water vapor pressure after Hardy (1998) to also be inline with dropsonde measurements processed with the ASPEN software), and recalculated the relative humidity after interpolation. The pressure is logarithmically interpolated.

We set data below XXX m to NAN in our level-3 data set. This value is consistent with the study by Yoneyama et al. (2002)
135 who found ship influences on radiosonde measurements to extend no further than 40 m above the deck.

3 Data characteristics

3.1 Ascending versus descending soundings

We begin with an examination of ascent and descent speeds for the different platforms (Fig. 3). The average ascent speed in
140 the mid-to-upper troposphere is between 4.5 and 5 ms^{-1} for radiosondes launched from the BCO, Atalante and MS-Merian.
(Fig. 3a,g,i).

Radiosondes launched from Meteor and RH-Brown ascend at slightly smaller rates of about 4 ms^{-1} (Fig. 3c,e).
For all platforms and at all altitudes the 10th and 90th percentiles are roughly symmetric about the mean ascent rate and fall
mostly within minus and plus, respectively, 1 ms^{-1} of the mean. Radiosondes from the Atalante and MS-Merian appear to
have experienced stronger updrafts in the upper troposphere. Above 20 km the mean ascent rate and the spread in ascent rates
increase for all platforms.

145 Descent speeds exhibit a much stronger functional dependence on altitude (Fig. 3b,d,f,h,j). For platforms that employed
parachutes (BCO, Meteor, Atalante and MS-Merian), descent rates decrease towards the ground to a minimum of about 5 ms^{-1}
in the lowest kilometers. Instruments without a parachute from RH-Brown have descent rates of slightly less than 15 ms^{-1}
in the lowest few kilometers. The positive skewness of the distributions associated with stations that used parachutes
is due to descending sondes with broken or detached parachutes. With the exponential decrease of air density with altitude,
150 descent rates increase non-linearly and rapidly with altitude, exceeding 20 ms^{-1} between 20–25 km when parachutes were
used and exceeding 40 ms^{-1} in case of the RH-Brown.

Fig. 4 compares the measurements of horizontal wind speed and air temperature between ascending and descending soundings.
It must be noted that this is not a perfect comparison for several reasons. First, as is evident from Fig. 6f, the instruments
drift substantial horizontal distances and thus, do not sample the same location. In addition, there are variable time-lags of the
155 order of a couple of hours between ascending and descending measurements. Finally, as quantified in Fig. 1, the number of
descent profiles available for computing statistics is in some cases substantially smaller than the number of ascent profiles.
These numbers of available measurements are shown on the right hand side of Fig. 4. For soundings from the BCO, Meteor,
RH-Brown and Atalante, the measurements of horizontal wind speeds are very similar between ascent and descent with nearly
identical standard deviations between ascent and descent at all levels. Yet, mean values of horizontal wind speeds above the
160 tropopause are slightly smaller for the descent compared to the ascent, and this effect is particularly pronounced for the RH-
Brown compared to BCO, Meteor and Atalante. This could suggest that excessively rapid descent rates introduce negative
biases in the horizontal wind-speed measurements. Finally, the mean profiles of horizontal wind speed derived from ascending
and descending soundings from the MS-Merian differ substantially. At 10–15 km altitude the difference in the mean has a

magnitude of about half the standard deviation of the descending profiles, and roughly a third of the standard deviation of the
165 ascending profiles, as the standard deviation is greater for ascending radiosondes. One plausible reason for the discrepancies in the profiles of MS-Merian soundings may be the relatively small number of recorded descents; at 12.5 km altitude, for instance, the number of ascending sondes is more than 3 times that of the descending sondes (Fig. 4f).

The comments we made regarding the comparison of horizontal wind speeds also apply to measurements of air temperature (Fig. 4b,d,f,h,j). For BCO, Meteor, RH-Brown and Atalante stratospheric temperature observations during descent are slightly
170 warmer than during ascent, and in case of the RH-Brown by more than one °C. This may again indicate a bias introduced by greater than optimum descent rates. As temperatures increase with altitude inside the stratosphere, we hypothesize that the sign of the bias is linked to an insufficient adjustment time of the temperatures sensor.

3.2 Observed conditions

As we pointed out with regard to Fig. 2, the radiosonde network during EUREC⁴A sampled well the latitude band around
175 Barbados, i.e., 12.5–14.5°N, but in addition the Atalante and MS-Merian collected data at latitude further to the south. Figure 5 compares the observed zonal and meridional winds, potential temperatures and mixing ratios between 12.5–14.5°N and 8.5–10.5°N for the period when there was data coverage at both locations (Jan 26–Feb 12). Colors show the occurrence frequencies or the difference in occurrence frequencies, respectively as a function of observed value (x-axis) and altitude (y-axis), a design inspired by the frequency-altitude-diagrams shown by Davison et al. (2013). The distributions of zonal wind speeds are very
180 similar between the northern and southern regions, with westerly winds at 6 km and 14 km altitude slightly stronger (by a few ms⁻¹) in the south. Larger differences exist in meridional winds; tropospheric northerlies are greater in the north with the exception of the lowest 3 km where they are stronger in the south.

The temperature gradient [CST: I will plot stability instead!] is greater in the south (potential temperatures in the upper half of the troposphere are warmer there while temperatures right above the tropopause are colder).

185 The greatest relative differences are found in the mixing ratios of water vapor, which are approximately twice as large in south between 3–8 km.

Figure 6 shows the temporal evolution of atmospheric conditions for the full period of data coverage averaged over the region north of 12.5°N. Results look nearly identical when only data from BCO are plotted (not shown). Before Jan 22 the mid-troposphere was relatively cool and zonal winds in the upper troposphere were strong. From Jan 22 onward the observational
190 domain experienced warmer temperatures , weaker upper-tropospheric westerlies as well as weaker easterlies near the surface. Positive pressure anomalies first appear in the upper troposphere and reach the surface at the end of January when a ridge started to dominate the area. Surface and upper-tropospheric winds started to strengthen again after Feb 6 while the positive pressure anomaly faded. A strong moistening of the mid and upper levels is seen around Feb 13 which coincides with a directional change of the meridional winds at these levels, favoring deeper cloud formation with cloud tops reaching up to 9km.

195 Figure 7 shows the temporal evolution of the vertical profiles of relative humidity for all radiosondes launched from the Meteor. The figure is based on level-three data (10 m vertical resolution) with time gaps filled by linear interpolation. During the descent of the soundings, the altitude at which the radio signal was lost ranged between 300-800 m. In order to recover

the near-surface values, we assume that temperature increases following a dry adiabat and that the water vapour mixing ratio is constant in a well-mixed boundary layer. Also shown is the predicted cloud base as estimated by the Lifting Condensation
200 Level (LCL) which we calculated with parcel theory from the sounding data. The LCL is compared to the observed cloud-base from the ceilometer on board. The ceilometer is a Jenoptik system that measures cloud-base fraction as a function of altitude, using LIDAR (light detection and ranging) technology, by detecting back-scattered returns from clouds and aerosols above the instrument at three different levels. All three levels form the ceilometer are represented simultaneously. The soundings-derived
205 is in excellent agreement with the cloud base height observed by the ceilometer. Multiple precipitation events were observed by the ceilometer for which the cloud base extends down to the surface. These events are well captured by the soundings, where they correspond to a lowered LCL. This is remarkable give that the temporal sampling period of the soundings is several times larger than the duration of the rain events. The presence of persistent high relative humidity values at the surface during and after precipitation is the explanation for this good agreement. Observed cloud tops align closely with the cores of supersaturation from the relative humidity profiles within the troposphere, ranging from about 2.0 km during shallow trade-cumuli regimes to
210 up to 15 km when cirrus clouds were present.

Many days during EUREC4A were characterized by sugar or, less frequently occurring, gravel clouds. Both types of convection are characterized by shallow boundary layer Cumulus clouds. Particularly on Feb 8-10th, both cloud types occurred, favored by easterly trade winds with surface winds varying around 8ms^{-1} . As seen in Fig. 7, the LCL for these days varied around 700m. The trade wind inversion was particularly well defined, separating the moist BL from the particularly dry free
215 troposphere. Clouds were shallow with cloud tops below 2000m, but occasionally reaching higher up to 3000m: these thicker clouds were often precipitating. Flower clouds, as described in Stevens et al. (2020) and Bony et al. as patches of Cumulus clouds with stratiform veils were observed on multiple days throughout EUREC4A. At BCO, these stratiform layers were most pronounced on Feb 2, Feb 5, Feb 12 and 13th.

Another cloud feature spanning over the whole northern observation region moved from the East of the region over BCO
220 between Jan 22-24. Following Stevens et al. (2020) and Bony et al., this mesoscale shallow cloud organisation pattern showed the characteristics of a Fish cloud. On these days, visible satellite images such as from GOES-E or MODIS on Aqua/Terra show the stratiform nature of this mesoscale convection pattern, as well as the surrounding cloud-free areas (see Fig. 8a)). Fig. 8b) illustrates the moistening of the atmosphere and the deepening of the BL throughout the event. Between Jan 20-26, the increase of integrated moisture up to 55kgm^{-2} nicely aligns with increasing BL top height, thus cloud top height and trade
225 wind inversion height. Before and after the event, this height is located around 2km, showing a mixture of Sugar and Gravel clouds; during the peak of the event on Jan 22nd and 23rd, marked by strong rain intensity of up to 15mmh^{-1} , the BL is deepened up to 5km height. During the passage of the Fish cloud pattern, the pressure in the BL was lowered by up to 4hPa (see Fig 6c)) and the temperature above the trade wind inversion between 6-8km showed a slight positive anomaly. Bony et al. found that this cloud feature often occurs under weaker surface trade wind speeds below 8ms^{-1} ; the sounding data confirms
230 this as the measured wind speeds in the northern latitude area lie well below this threshold in the lower boundary layer.

3.2.1 HEADING

TEXT

4 Conclusions

TEXT

235 5 Code availability

TEXT

6 Data availability

TEXT

7 Code and data availability

240 TEXT

Sample availability. TEXT

Video supplement. TEXT

Appendix A: Extra soundings onboard the Atalante

- MeteoModem: Meteo Modem sondes reached 10 km height, these used 150 g balloons. Vaisala: 200 and 350g. MeteoModem: – software version: Eoscan build 1.2.190205 – Station: Upper Air sounding system SR10 – M10GPSonde radiosonde – M10GPSondes calibration deck – GPS antenna, omnidirectional UHF antenna, turnstile antenna for subtropical regions. For the MeteoModem RS, a set of frequencies (400.4, 400.6, 401.8, 402.4, 402.8, 403.2, and 403.4 MHz) was used to prevent any interference between the different launchings. As each MeteoModem RS was stopped at 10 km high, this led to have up to 5 emitted frequencies at the same time during intensive radiosounding phases.
- 250 11 MeteoModem RS were launched during a Transect of Intensive Radiosounding (TIR1, Eddy 1) on the 26th January 2020. 2 others were launched in the center of the warm core of Eddy 2 on the 27th January 2020 (Eddy 1 was a smaller eddy with no clear SST signature). 29 Meteomodem sondes were launched during a second Transect of Intensive Radiosounding (TIR2)

from the 02nd to the 03rd February 2020. Another Meteomodem sonde was launched during a station under an important convective system the 10th February 2020). 4 RS were done under cloud streets (TIR3) on the 17th february 2020. Two sondes
255 did not pass the calibration tests.

An issue was detected in the files of the MeteoModem RS. At the first level, the dew point value is set to the air temperature. This bias will be corrected after the end of the cruise. The NetCDF files generated were send to the aeris portal with a readme file pointing out this issue.

A1

260 *Author contributions.* TEXT

Competing interests. TEXT

Disclaimer. TEXT

Acknowledgements. Special thanks to Angela Gruber.

References

- 265 Bony, S., Schulz, H., Vial, J., and Stevens, B.: Sugar, Gravel, Fish and Flowers: Dependence of Mesoscale Patterns of Trade-wind Clouds
on Environmental Conditions, *Geophysical Research Letters*, n/a, <https://doi.org/10.1029/2019GL085988>, <https://agupubs.onlinelibrary.wiley.com/doi/abs/10.1029/2019GL085988>.
- Davison, J. L., Rauber, R. M., Di Girolamo, L., and LeMone, M. A.: A Revised Conceptual Model of the Tropical Marine Boundary Layer.
Part I: Statistical Characterization of the Variability Inherent in the Wintertime Trade Wind Regime over the Western Tropical Atlantic, *J.*
270 *Atm. Sci.*, 70, 3005–3024, <https://doi.org/10.1175/JAS-D-12-0321.1>, 2013.
- Hardy, B.: ITS-90 formulations for vapor pressure, frostpoint temperature, dewpoint temperature, and enhancement factors in the range –100
to + 100 C, in: *The Proceedings of the Third International Symposium on Humidity & Moisture*, Teddington, London, England, pp. 1–8,
1998.
- 275 Stevens, B., Bony, S., Brogniez, H., Hentgen, L., Hohenegger, C., Kiemle, C., L'Ecuyer, T. S., Naumann, A. K., Schulz, H., Siebesma, P. A.,
Vial, J., Winker, D. M., and Zuidema, P.: Sugar, gravel, fish and flowers: Mesoscale cloud patterns in the trade winds, *Quarterly Journal of*
the Royal Meteorological Society, 146, 141–152, <https://doi.org/10.1002/qj.3662>, <https://rmets.onlinelibrary.wiley.com/doi/abs/10.1002/qj.3662>, 2020.
- Yoneyama, K., Hanyu, M., Sueyoshi, S., Yoshiura, F., and Katsumata, M.: Radiosonde observation from ships in the tropical region, *JAM-*
STECR, 45, 2002.

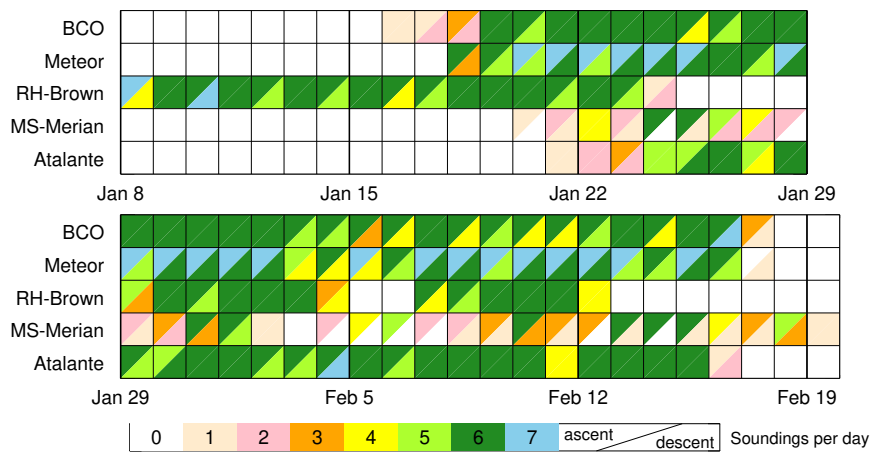


Figure 1. Daily number of ascending and descending, respectively, soundings associated with each platform.

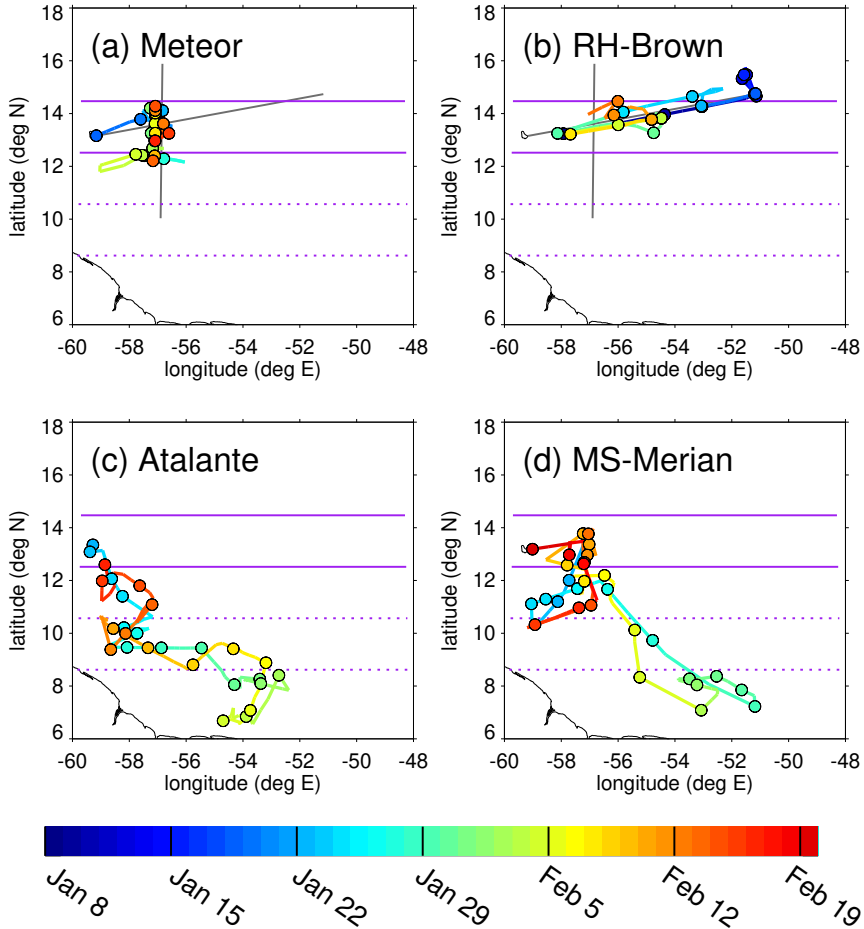


Figure 2. Routes and launch coordinates of radiosondes for the four research vessels, colored by date. Circles mark the locations of the first radiosonde launch on each day. The gray lines in (a) and (b) mark the nearly orthogonal lines that were sampled by Meteor (North-South) and RH-Brown (West-East). Purple lines mark the northern ($12.5\text{--}14.5^\circ\text{N}$; solid) and southern ($8.5\text{--}10.5^\circ\text{N}$; dashed) latitude bands that we use for a comparison of radiosonde measurements in Fig. 5.

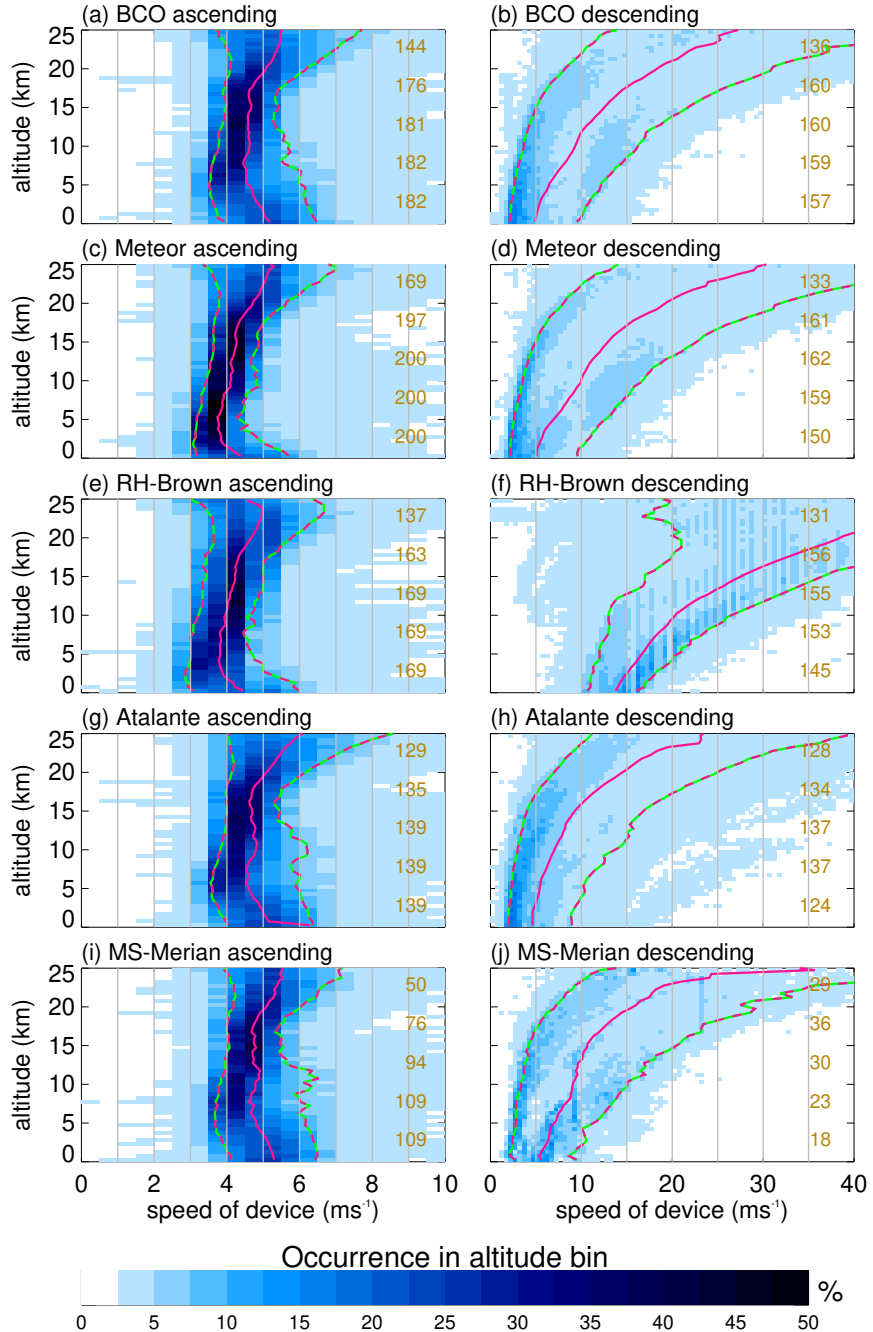


Figure 3. Instrument (left) ascent and (right) descent speeds as a function of height. The sum of occurrence frequencies in each altitude bin is 100%. The pink line shows the mean profiles and the pink-green lines show the 10th and the 90th percentiles, respectively. Altitude bins are 500 m deep and speed bins are 0.5 ms^{-1} wide. The numbers of sondes that crossed the corresponding height-levels (2.5, 7.5, 12.5, 17.5 and 22.5 km, respectively) are shown in each panel.

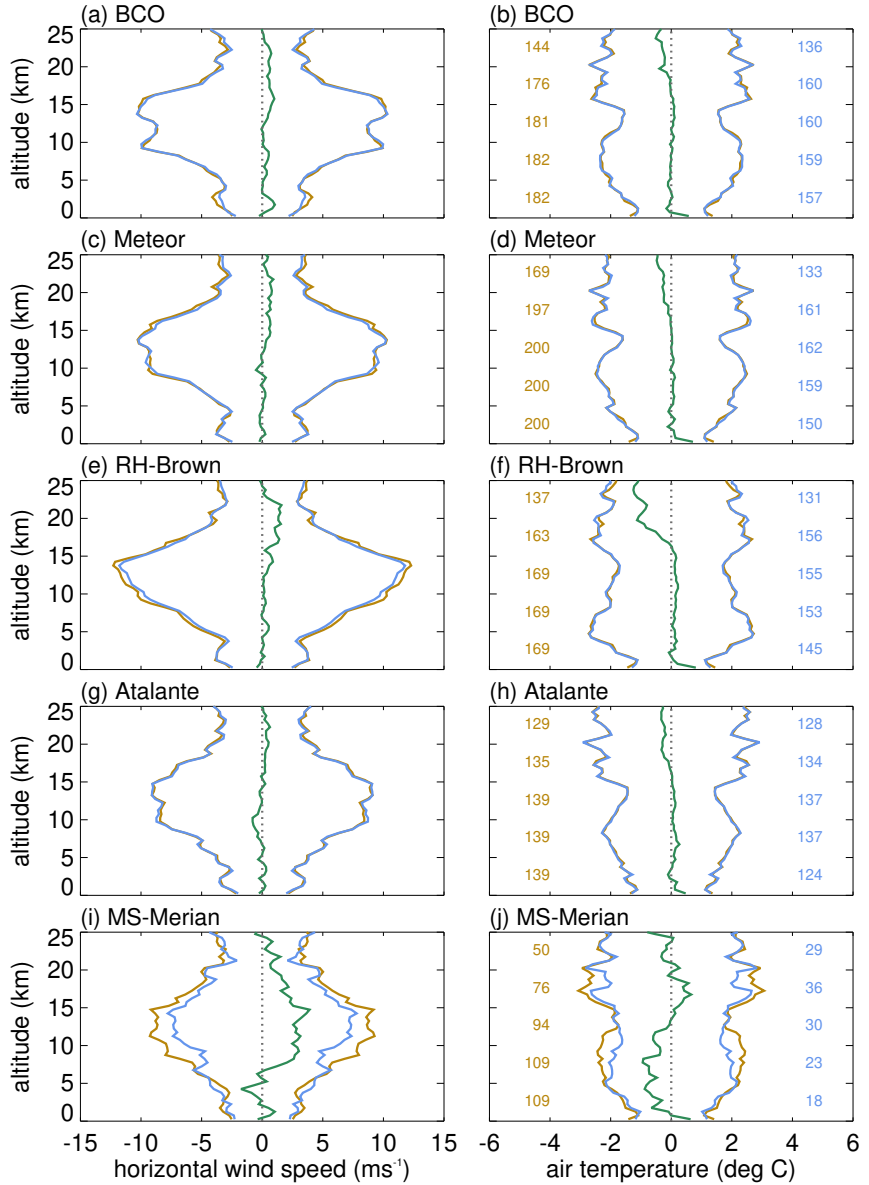


Figure 4. Comparison of (left) horizontal wind speed and (right) air temperature measured during ascent and descent. The green lines show the time-averaged values during ascent minus the time-averaged values during decent. The brown (blue) lines show ±1 standard deviation for ascent (descent). Numbers inside the panels on the right-hand side show the counts of ascending (brown) and descending (blue) sondes that crossed the corresponding height-levels (2.5, 7.5, 12.5, 17.5 and 22.5 km, respectively.)

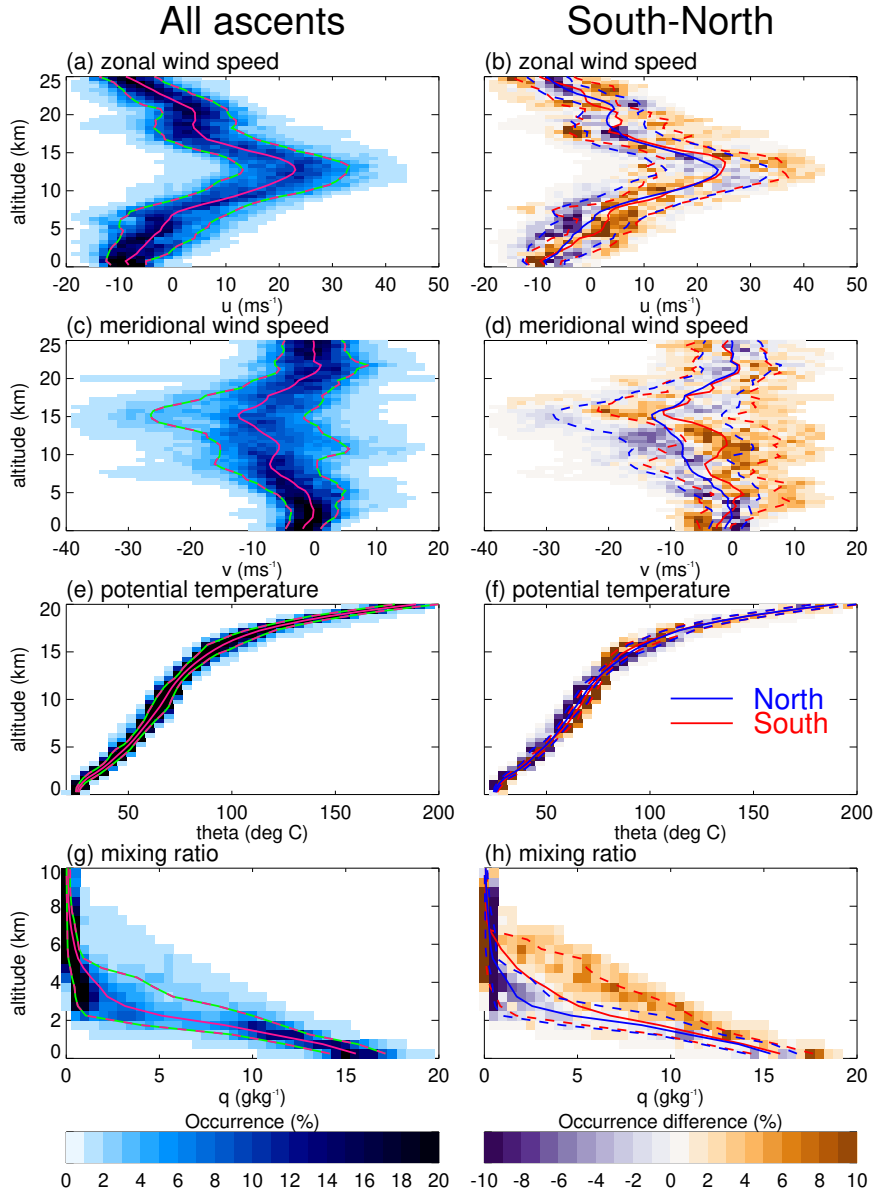


Figure 5. Occurrences of (a) zonal wind speed, (c) meridional wind speed, (e) potential temperature and (g) water vapor mixing ratio as a function of height for all soundings launched between Jan 26 and Feb 12 (437 profiles). The sum of occurrence frequencies in each altitude bin is 100%. The pink lines show the mean profiles and the pink-green lines show the 10th and the 90th percentiles, respectively. Altitude bins are 500 m deep and each x-axis contains 40 bins. (b,d,f,h) show differences in occurrences between the southern (8.5–10.5°N, 63 profiles) and northern (12.5–14.5°N; 261 profiles) latitude bands, which are marked in Fig. 2. They are obtained by computing diagrams such as (a,c,e,g) for each region separately and subtracting them afterwards. Solid lines in (b,d,f,h) show the mean profiles in each region and dashed lines the 10th and the 90th percentiles. All data use ascending profiles.

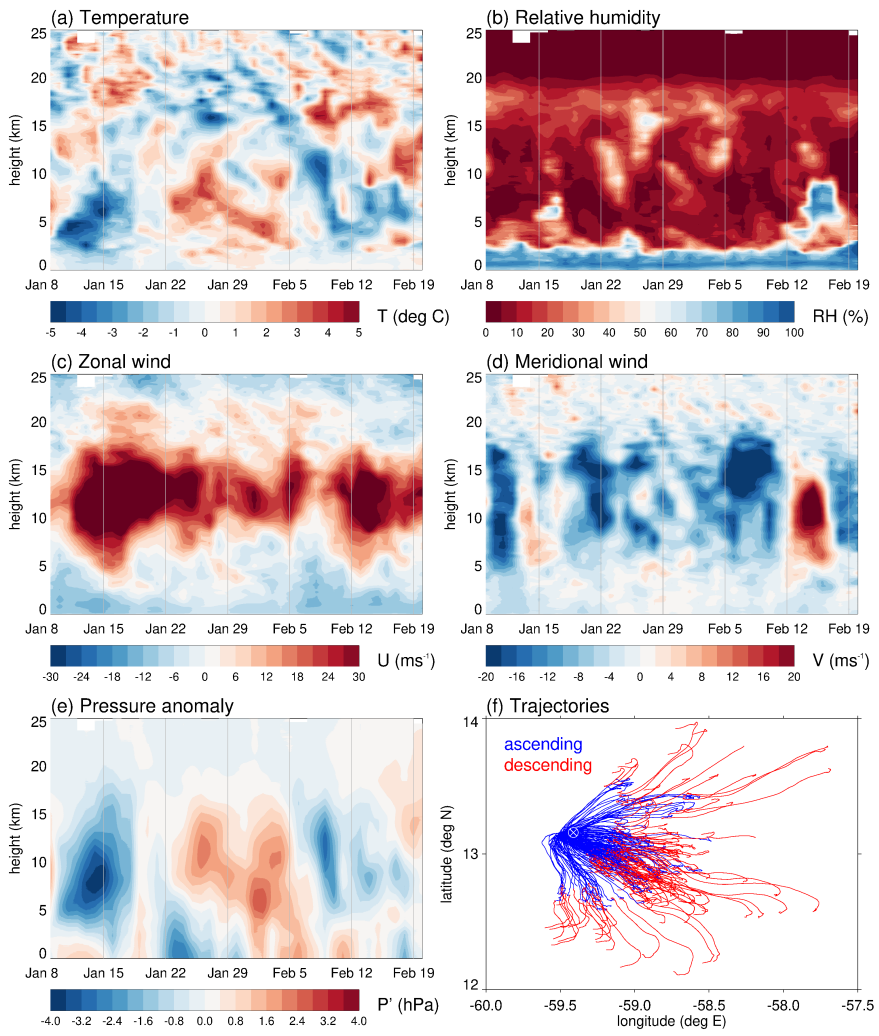


Figure 6. (a-e) Time-height cross sections of daily (a) temperature anomaly, (b) relative humidity, (c) zonal wind, (d) meridional wind and (e) pressure anomaly computed from ascending soundings north of 12.5°N . The data combine 182 soundings from the BCO, 169 from the RH-Brown, 150 from the Meteor, 28 from the MS-Merian and 4 from the Atalante. Anomalies are defined as deviations from the time-average at each altitude. (f) The horizontal trajectories of ascending and descending, respectively, radiosondes launched from the BCO.

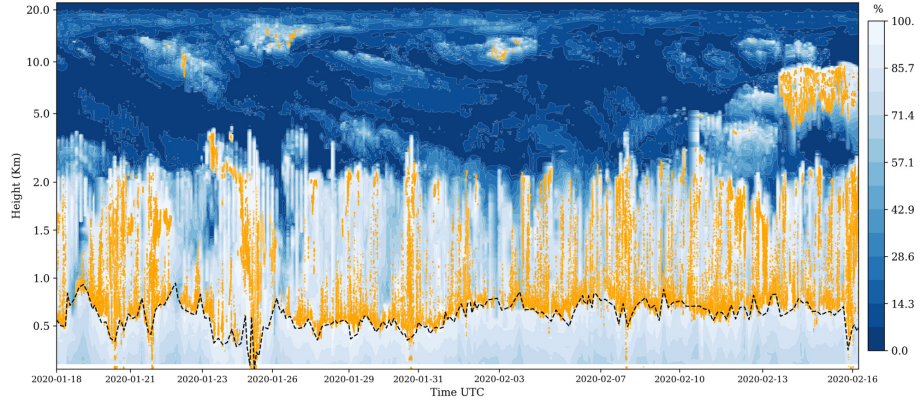


Figure 7. Comparison between ascending soundings and ceilometer measurements on the Meteor. The relative humidity from radiosonde measurements is shown in blue to white shading. The black dashed line represents the Lifting Condensation Level calculated from surface values using thermodynamic parcel theory. Clouds, as observed by the ceilometer, are marked with orange dots. The vertical axis is chosen to be logarithmic for better visibility of the moisture distribution near the surface. The time-axis for the soundings uses launch time. The temporal resolution of the ceilometer data is 10 s.

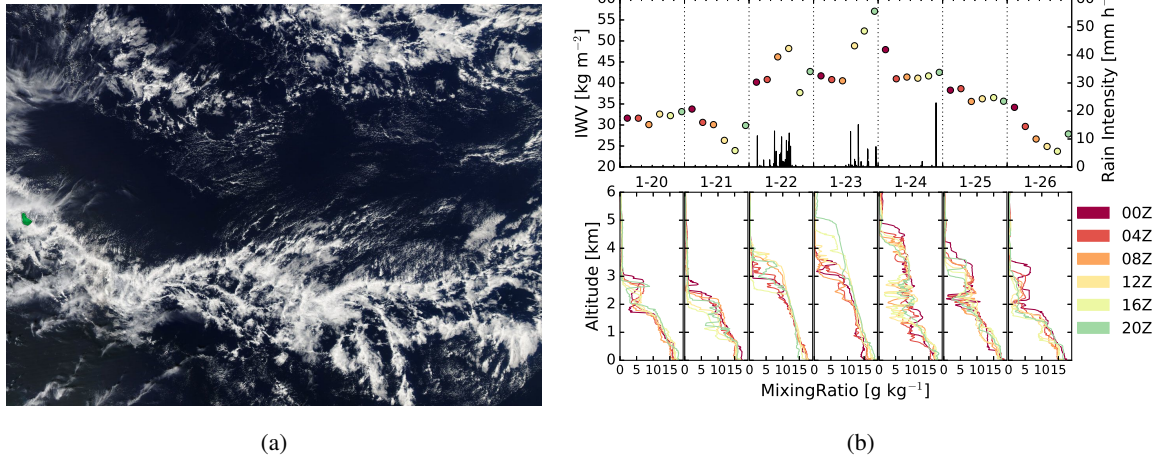


Figure 8. Fish cloud pattern passing Barbados between 22. - 24.01.2020. (a) MODIS-Aqua scene from 22.01.20, image covering $9\text{--}18^{\circ}\text{N}$, $48\text{--}60^{\circ}\text{W}$ with Barbados shown in artificial green. (b) Temporal Evolution of Mixing Ratio (lower panel) and IWV (upper panel) as measured by the BCO soundings January 20 - 26. Profiles and calculated IWV values are color-coded by times of soundings reaching 100hPa. The upper panel also shows the rain intensity as measured at BCO.

Table A1. For each platform the rows list (1) the numbers of recorded ascending soundings, (2) the numbers of recorded descending soundings, (3) the first date of data coverage, (4) the last date of data coverage, (5) whether or not parachutes were used, (6) the Vaisala MW41 software version, (7) the station altitude relative to sea level, (8) the GPS antenna offset relative to the station, (9) the Launch site offset relative to the station, (10) the surface barometer offset relative to the station, (11) the frequency used to transmit the signal from the sonde to the antenna, (12) whether or not it was attempted to transmit data to the Global Telecommunication System.

| | BCO | Meteor | RH-Brown | Atalante | MS-Merian |
|------------------------------|----------------|----------------|----------|-----------|----------------|
| Number ascents | 182 | 200 | 169 | 139 | 111 |
| Number descents | 160 | 162 | 157 | 137 | 37 |
| Start date | Jan 16 | Jan 18 | Jan 8 | Jan 21 | Jan 20 |
| End date | Feb 17 | Feb 17 | Feb 12 | Feb 16 | Feb 19 |
| Use of parachutes | yes | yes | no | yes | yes |
| Software version | 2.15 2.15.0-37 | 2.15 2.15.0-37 | 2.2.15 | 2.15.2-42 | 2.15 2.15.0-37 |
| Station altitude (msl) | 25.0 | 18.0 | 4.3 | 13.1 | 10.4 |
| GPS antenna offset (m) | 4.3 | 2.0 | 5.5 | 2.6 | 1.6 |
| Launch site offset (m) | 0.0 | -8.0 | 0.5 | -0.6 | 0.0 |
| Surface barometer offset (m) | 1.0 | 1.2 | -4.3 | 0.2 | 0.6 |
| Frequency (MHz) | 400.2 | 401.5 | 400.5 | 401.2 | 403.0 |
| Transmission to GTS | yes | no | yes | yes | no |